Path-Integral Monte Carlo Determination of the Fourth-Order Virial Coefficient for a Unitary Two-Component Fermi Gas with Zero-Range Interactions

Yangqian Yan and D. Blume
Department of Physics and Astronomy, Washington State University, Pullman, Washington 99164-2814, USA
(Received 6 February 2016; published 7 June 2016)

The unitary equal-mass Fermi gas with zero-range interactions constitutes a paradigmatic model system that is relevant to atomic, condensed matter, nuclear, particle, and astrophysics. This work determines the fourth-order virial coefficient b_4 of such a strongly interacting Fermi gas using a customized *ab initio* path-integral Monte Carlo (PIMC) algorithm. In contrast to earlier theoretical results, which disagreed on the sign and magnitude of b_4, our b_4 agrees within error bars with the experimentally determined value, thereby resolving an ongoing literature debate. Utilizing a trap regulator, our PIMC approach determines the fourth-order virial coefficient by directly sampling the partition function. An on-the-fly antisymmetrization avoids the Thomas collapse and, combined with the use of the exact two-body zero-range propagator, establishes an efficient general means to treat small Fermi systems with zero-range interactions.

DOI: 10.1103/PhysRevLett.116.230401

Introduction.—Strongly interacting Fermi gases manifest themselves in nature in different forms, from neutrons in neutron stars [1] to electrons in solids [2]. These systems are generally deemed difficult to treat theoretically because of the lack of a small interaction parameter. Superconductivity [3] and exotic states such as fractional quantum hall [4] or Fulde-Ferrell-Larkin-Ovchinnikov [5–7] states have been observed or predicted to exist in these systems. Ultracold Fermi gases [8,9], which can nowadays be produced routinely in tabletop experiments, are ideal for studying strongly interacting systems since (i) the van der Waals interaction is short ranged, which means that it can be approximated by a contact potential that introduces a single length scale, i.e., the s-wave scattering length a_s; and (ii) a_s can be tuned at will utilizing Feshbach resonance techniques [10]. When a_s diverges, i.e., becomes infinitely large, the two-body contact potential does not define a length scale [11]. Just like the noninteracting Fermi gas, the properties of the unitary Fermi gas (Fermi gas with infinite a_s) are determined by two length scales, the de Broglie wavelength λ and interparticle spacing $\bar{r}$ [12].

At high temperature, λ is much smaller than $\bar{r}$ and the grand canonical thermodynamic potential Ω can be expanded in terms of the fugacity [13,14]. The nth-order expansion or virial coefficient b_n is determined by the partition functions of clusters containing n or fewer fermions. Since all thermodynamic properties at high temperature can be derived from the virial coefficients b_n [15], the b_n's are essential to understanding the normal state of strongly interacting Fermi gases.

While the second- and third-order virial coefficients are well understood [13,15–21], none of the theoretical calculations for b_4 [22–25] agree with the experimental data [19,26]. This Letter rectifies this situation: our theoretically determined b_4 agrees with the experimentally determined value. Our approach uses a trap regulator [27,28] and employs the path-integral Monte Carlo (PIMC) technique [29,30], with the contact interactions incorporated exactly via the two-body zero-range propagator [31]. The "post-antisymmetrization" [29,30], traditionally employed in PIMC calculations, does not work for the system with zero-range interactions, since the sampled paths shrink due to the Thomas collapse, a well-known phenomenon for bosons [32,33], to a single point. For bosons, the three-body Thomas collapse is cured by introducing an additional scale or three-body parameter [33]. For fermions, such a three-body parameter is not needed since the Pauli exclusion principle acts as an effective three-body repulsion [34,35]. Thus, rather than the standard "post-antisymmetrization", we use an "on-the-fly scheme" [36,37], which antisymmetrizes at each imaginary time step. While the antisymmetrization is, within Monte Carlo frameworks, usually associated with the infamous Fermi sign problem [38–40], in our case, it stabilizes the simulation and affords the use of significantly smaller number of time slices than the use of finite-range interactions would. Our approach reproduces the trap regulated b_3 over a wide temperature range. We determine the trap regulated b_4 as a function of the temperature T. In the low-temperature regime, we find agreement with Ref. [22]. We separate the spin-balanced ($b_{2,2}/2$) and spin-imbalanced ($b_{3,1}$) subcluster contributions to b_4, $b_4 = b_{3,1} + b_{2,2}/2$, and find $b_{2,2} < 0$ and $b_{3,1} > 0$ at all considered temperatures. $b_{2,2}$ dominates at low T and $b_{3,1}$ at high T. Converting the trap regulated virial coefficient b_4 to that of the homogeneous system using the local density approximation (LDA) [16], we find agreement with the experimentally determined values [19,26].

Virial expansion framework.—The nth-order virial coefficient b_n^{hom} of the homogeneous system at unitarity is

related to the high-temperature limit b_n^0 of the harmonically trapped unitary system via $b_n^{\rm hom} = n^{3/2} b_n^0$ [16,28]. To determine b_n^0, we calculate the virial coefficient b_n of the harmonically trapped system for various temperatures and then take the $T \to \infty$ limit. The trap Hamiltonian $H(n_1, n_2)$ for n_1 particles of species 1 and n_2 particles of species 2 with interspecies s-wave interactions reads

$$H(n_1,n_2) = \sum_{j=1}^{n_1+n_2} \left(\frac{-\hbar^2}{2m} \nabla_{\mathbf{r}_j}^2 + \frac{1}{2} m\omega^2 \mathbf{r}_j^2 \right) + \sum_{i=1}^{n_1} \sum_{j=n_1+1}^{n_1+n_2} V_{2b}(\mathbf{r}_i - \mathbf{r}_j), \quad (1)$$

where m denotes the mass of the particles, $\mathbf{r}_j$ the position vector of the jth particle, ω the angular trapping frequency, and V_{2b} the regularized Fermi-Huang pseudopotential with infinite a_s [41]. The grand canonical thermodynamic potential Ω can be written in terms of the fugacities z_i of species i,

$$\Omega = -k_B T \ln \left(\sum_{n_1=0}^{\infty} \sum_{n_2=0}^{\infty} Q_{n_1,n_2} z_1^{n_1} z_2^{n_2} \right), \quad (2)$$

where z_i is equal to $\exp[\mu_i/(k_B T)]$, μ_i is the chemical potential of species i, and Q_{n_1,n_2} is the canonical partition function for $H(n_1, n_2)$,

$$Q_{n_1,n_2} = \mathrm{Tr}\, \exp\left[-H(n_1,n_2)/(k_B T)\right]. \quad (3)$$

Here, Tr is the trace operator. Defining $\Delta\Omega = \Omega - \Omega^{\rm ni}$, where $\Omega^{\rm ni}$ is the grand canonical potential of the noninteracting system, and Taylor-expanding around $z_1 = z_2 = 0$ [42,43], one finds

$$\Delta\Omega = -k_B T Q_{1,0} \left(\sum_{n_1=1}^{\infty} \sum_{n_2=1}^{\infty} b_{n_1,n_2} z_1^{n_1} z_2^{n_2} \right). \quad (4)$$

For spin-balanced systems, z_1 and z_2 are equal, and Eq. (4) reduces to

$$\Delta\Omega = -2 k_B T Q_{1,0} \left(\sum_{n=2}^{\infty} b_n z^n \right), \quad (5)$$

where $b_2 = b_{1,1}/2$, $b_3 = (b_{1,2} + b_{2,1})/2$, and $b_4 = (b_{1,3} + b_{3,1} + b_{2,2})/2$ (note, one has $b_{2,1} = b_{1,2}$ and $b_{3,1} = b_{1,3}$). It is convenient to write the virial coefficients b_{n_1,n_2} as

$$b_{n_1,n_2} = \Delta b_{n_1,n_2} + b_{n_1,n_2}^{\rm ref}, \quad (6)$$

where $b_{n_1,n_2}^{\rm ref}$ is determined by the virial coefficients b_{j_1,j_2} and the canonical partition functions Q_{j_1,j_2} with $j_1 + j_2 < n_1 + n_2$. The term $\Delta b_{n_1,n_2} = (Q_{n_1,n_2} - Q_{n_1,n_2}^{\rm ni})/Q_{1,0}$, where $Q_{n_1,n_2}^{\rm ni} = Q_{n_1,0} Q_{0,n_2}$, in contrast, accounts for the "new" physics introduced by the interacting (n_1, n_2) clusters [44].

Contradicting literature results for b_4.—The literature results are summarized in Table I (see also the Supplemental Material [45]). Two independent experiments find consistent values for the fourth-order virial coefficient. The theoretical literature results, however, disagree with these experimental results, reflecting the fact that the fourth-order problem is highly nontrivial analytically and numerically. Using a sum-over-states approach with an energy cutoff, Ref. [22] obtained the low-temperature behavior of b_4. Assuming a monotonic temperature dependence and extrapolating to the $T \to \infty$ limit, Ref. [22] obtained b_4^0. It was concluded that more four-body energies would need to be calculated explicitly to obtain b_4 reliably at high temperature. The fourth-order virial coefficient has also been obtained by a diagrammatic approach, which included only a subset of the four-body free-space diagrams [23], and by applying a conjecture inspired by three-body results [24,25].

Customized PIMC algorithm.—$\Delta b_{n_1,n_2}$ is determined by the partition function Q_{n_1,n_2} of the interacting (n_1, n_2) system (Q_{n_1,n_2} is not known in general) and the partition function $Q_{n_1,n_2}^{\rm ni}$ of the noninteracting (n_1, n_2) system ($Q_{n_1,n_2}^{\rm ni}$ is known analytically). We calculate the ratio of the partition functions $Q_{n_1,n_2}^{\rm ni}/Q_{n_1,n_2}$ using the PIMC technique. Specifically, the simulation generates configurations according to Q_{n_1,n_2} and accumulates the ratio $Q_{n_1,n_2}^{\rm ni}/Q_{n_1,n_2}$ as a weight. The reason for using the partition function of the unitary Fermi gas and not that of the

TABLE I. Summary of literature and PIMC results.

$b_4^{\rm hom}$	b_4^0	Reference	Comment
0.096(15)	0.01200(188)	[19]	ENS experiment
0.096(10)	0.01203(125)	[26]	MIT experiment
−0.016(4)	−0.0020(5)	[22]	Sum-over-states approach
0.06	0.0075	[23]	Diagrammatic approach
−0.063(1)	−0.007875(125)	[24]	3-body inspired conjecture
0.078(18)	0.0098(23)		PIMC, this work

noninteracting gas as the "guiding function" is the following. The probability density to find two unlike particles with vanishing interparticle spacing is finite at unitarity and zero in the noninteracting limit. If we used $Q^{\rm ni}_{n_1,n_2}$ as the guiding function, configurations in which two unlike particles are at the same spatial position would be absent and the standard deviation of $Q_{n_1,n_2}/Q^{\rm ni}_{n_1,n_2}$ would be infinite, rendering the expectation value meaningless [46].

In the PIMC formulation, the partition function $Q^{\rm Boltz}_{n_1,n_2}(\beta)$ for Boltzmann particles (no exchange symmetries) at inverse temperature β, $\beta = (k_B T)^{-1}$, is written in terms of a product over density matrices at imaginary time τ,

$$Q^{\rm Boltz}_{n_1,n_2}(\beta) = \int \cdots \int \prod_{i=1}^{N} \rho(\mathbf{R}_i, \mathbf{R}_{i+1}; \tau) d\mathbf{R}_1 \cdots d\mathbf{R}_N, \tag{7}$$

where $\mathbf{R}_i$ collectively denotes the particle configurations at time slice i, $\mathbf{R}_{N+1} = \mathbf{R}_1$, and $N = \beta/\tau$. For the two-component Fermi gas, the standard PIMC approach writes the partition function as $Q_{n_1,n_2} = \mathcal{A} Q^{\rm Boltz}_{n_1,n_2}$, where $\mathcal{A}$ is the antisymmetrizer [29,47]. For the two-component Bose gas, the antisymmetrizer $\mathcal{A}$ is replaced by the symmetrizer $\mathcal{S}$. $\mathcal{A}$ and $\mathcal{S}$ contain the same number and types of terms; however, while all terms in $\mathcal{S}$ enter with a plus sign, $\mathcal{A}$ contains alternating plus and minus signs. Since the symmetrizer and antisymmetrizer are, in the standard PIMC approach, evaluated stochastically, the two-component Fermi and Bose gases are simulated using the same paths. Expectation values, however, are accumulated with plus and minus signs for fermions and with plus signs only for bosons. We refer to this standard approach as post-symmetrization. The bosonic system with interspecies two-body zero-range interactions but without a three-body regulator would collapse to a single point; this is the well-known Thomas collapse [32]. Correspondingly, the fermionic paths would also collapse, rendering the simulation meaningless. To get around this problem, we developed a customized on-the-fly antisymmetrization scheme, which explicitly antisymmetrizes the density matrix at each imaginary time step,

$$Q_{n_1,n_2}(\beta) = \int \cdots \int \prod_{i=1}^{N} \mathcal{A}\rho(\mathbf{R}_i, \mathbf{R}_{i+1}; \tau) d\mathbf{R}_1 \cdots d\mathbf{R}_N. \tag{8}$$

The observable is then calculated using

$$\frac{Q^{\rm ni}_{n_1,n_2}}{Q_{n_1,n_2}} = \left\langle \prod_{i=1}^{N} \frac{\mathcal{A}\rho^{\rm ni}(\mathbf{R}_i, \mathbf{R}_{i+1}; \tau)}{\mathcal{A}\rho(\mathbf{R}_i, \mathbf{R}_{i+1}; \tau)} \right\rangle, \tag{9}$$

where $\rho^{\rm ni}$ denotes the density matrix for the noninteracting system and $\langle \ldots \rangle$ the thermal average using paths generated for the unitary Fermi gas using the on-the-fly antisymmetrization scheme. Our simulation uses the pair-product approximation [29,45] with the exact two-body density matrix for zero-range interactions. The on-the-fly scheme employed here is related to earlier works [36,48], which antisymmetrized, as we do, at each time slice. The key difference is that we employ a density matrix that accounts for the interactions while the earlier works employed the noninteracting density matrix together with the Trotter (or improved Trotter) formula.

The on-the-fly antisymmetrization scheme treats the $n_1!n_2!$ permutations explicitly at each time slice, eliminating the need of the standard stochastic "permute move". As a consequence, the scheme is computationally prohibitively demanding for large systems. For small systems, however, it is quite efficient for three reasons: (i) The number of permutations is manageable for small $n_1 + n_2$. (ii) The use of the zero-range interactions eliminates the need to perform calculations for several different ranges of the underlying two-body potential. (iii) Compared to finite-range interactions [49], the number of time slices needed to reach convergence for the zero-range interacting systems considered here is rather small; e.g., our scheme yields $Q^{\rm ni}_{3,1}/Q_{3,1}$ at $E_{\rm ho}/(k_B T) = 0.8$ with 0.1% error using only $N = 9$ imaginary time slices (here, $E_{\rm ho} = \hbar\omega$). Within our approach, the key challenge in determining b_4 reliably at high temperature comes from the fact that $\Delta b_{2,2}$, $\Delta b_{3,1}$, $b^{\rm ref}_{2,2}$, and $b^{\rm ref}_{3,1}$ diverge, to leading order, as $(k_B T/E_{\rm ho})^6$. This implies that $b_{2,2}$ and $b_{3,1}$ are, at high temperature, obtained by adding two numbers of opposite sign and nearly equal magnitude. Thus, to obtain reliable values at high temperature, we need to determine our observables with high accuracy. In practice, our available computer time limits us to $k_B T \leq 2E_{\rm ho}$ for the (2,2) and (3,1) systems.

PIMC results.—To benchmark our customized PIMC algorithm, we apply it to the (2,1) system at unitarity, for which $Q^{\rm ni}_{2,1}/Q_{2,1}$ and b_3 can be calculated with high accuracy for all temperatures using the sum-over-states approach [16]. As an example, circles in Fig. 1(a) show the quantity $Q^{\rm ni}_{2,1}/Q_{2,1}$ for $k_B T = E_{\rm ho}$, obtained using our PIMC algorithm, as a function of the imaginary time step τ. The τ considered correspond to between $N = 4$ and 10 time slices. The simulation is exact in the $\tau \to 0$ (or equivalently, $N \to \infty$) limit. To extrapolate to the $\tau \to 0$ limit, we fit a fourth-order polynomial of the form $a + b\tau^2 + c\tau^4$ to the PIMC data [solid line in Fig. 1(a)]. Our extrapolated result of 0.499989(26) agrees within error bars with the value of 0.500014 [dashed line in Fig. 1(a)] obtained by the sum-over-states approach. Using the extrapolated $\tau \to 0$ values for $Q^{\rm ni}_{2,1}/Q_{2,1}$ at various temperatures T, we obtain b_3 as a function of T [circles in Fig. 1(b)]. The agreement with the sum-over-states results [solid line in Fig. 1(b)] is excellent for all T considered, demonstrating the reliability and accuracy of our PIMC approach.

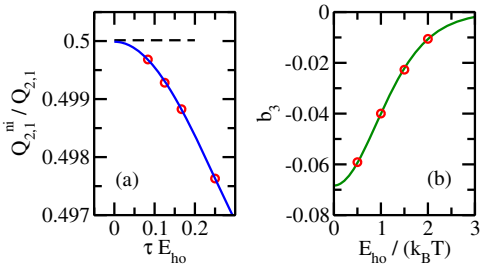

FIG. 1. Benchmarking our PIMC results (circles) for the (2,1) system at unitarity through comparison with sum-over-states results. (a) The observable $Q_{2,1}^{\mathrm{ni}}/Q_{2,1}$ as a function of the imaginary time step τ at $k_BT = E_{\mathrm{ho}}$. The circles show our PIMC results. The error bars (not shown) are smaller than the symbol size. The solid line shows the fourth-order polynomial fit of the form $a + b\tau^2 + c\tau^4$. The dashed line shows the sum-over-states results. (b) b_3 as a function of $1/(k_BT)$. The circles show our PIMC results while the solid line shows the sum-over-states results.

We now discuss the determination of b_4. The extrapolation of the raw data to the $\tau \to 0$ limit is discussed in the Supplemental Material [45]. Circles in Figs. 2(a) and 2(b) show our PIMC results for $b_{3,1}$ and $b_{2,2}$, respectively, as a function of the inverse temperature. At low temperature, the PIMC results agree with the sum-over-states results (solid lines), obtained using the data provided in Ref. [22]. At all temperatures, $b_{3,1}$ is positive and $b_{2,2}$ is negative. It has been shown that $b_{1,1}$ and $b_{2,1}$ are even functions of $E_{\mathrm{ho}}/(k_BT)$ [16,20,43], and the conjecture of Ref. [25] implies that $b_{3,1}$ and $b_{2,2}$ are also even functions of $E_{\mathrm{ho}}/(k_BT)$. Thus, to obtain $b_{3,1}$ and $b_{2,2}$, we fit the data for the four highest temperatures to the form $a + b[E_{\mathrm{ho}}/(k_BT)]^2$. The dashed lines in Figs. 2(a) and 2(b) show the fits. Since the data at $k_BT = 2E_{\mathrm{ho}}$ have much larger error bars than those at lower temperatures, the data contribute comparatively little to the fit, which weighs each data point by the inverse of the square of its error bar. We find $b_{3,1}^0 = 0.0212(8)$ and $b_{2,2}^0/2 = -0.0115(8)$, where the error bars reflect the uncertainty of the fit. We unfortunately do not have sufficiently many data to include a $(k_BT)^{-4}$ term in the fit. Since the inclusion of a $(k_BT)^{-4}$ term in the fit could alter the $T \to \infty$ result, we add an *ad hoc* systematic error of 0.0008 to $b_{3,1}^0$ and $b_{2,2}^0/2$, yielding $b_{3,1}^0 = 0.0212(16)$ and $b_{2,2}^0/2 = -0.0115(16)$ [crosses in Figs. 2(a) and 2(b)]. To obtain b_4 [see Fig. 2(c)], we combine $b_{3,1}$ and $b_{2,2}$. Specifically, the circles and the fit are obtained by adding the data of Figs. 2(a) and 2(b) while the error bar of the cross at $T \to \infty$ is obtained using standard error propagation. b_4 displays an interesting temperature dependence: It is negative at low temperature due to the dominance of $b_{2,2}$, vanishes at $k_BT \approx E_{\mathrm{ho}}$ due to a cancellation of $b_{3,1}$ and $b_{2,2}/2$, and is positive at high temperature due to the dominance of $b_{3,1}$. Our results resolve the discrepancy of the sign of b_4 between Ref. [22] and the experiments [19,26]. Our extrapolated b_4 at infinite temperature is $b_4^0 = 0.0098(23)$, which agrees with the experimental results of $b_4^0 = 0.01203(125)$ [26] [diamond in Fig. 2(c)] and $b_4^0 = 0.01200(188)$ [19] (see also Table I). Using the LDA, we find $b_4^{\mathrm{hom}} = 0.078(18)$.

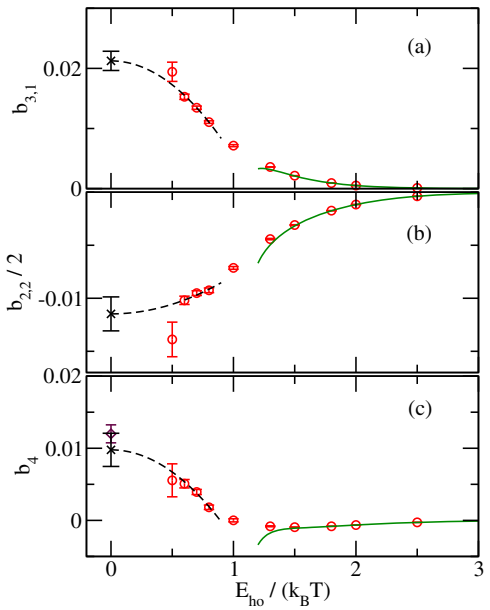

FIG. 2. PIMC determination of the fourth-order virial coefficient. Circles in panels (a), (b), and (c) show $b_{3,1}$, $b_{2,2}/2$, and b_4, respectively, determined by our PIMC approach. The crosses in (a) and (b) show the $T \to \infty$ limit of the two-parameter fit (dashed line) to the PIMC data at the four highest temperatures. The dashed line and the cross in (c) show the sum of the fits from (a) and (b). The error bar in (c) is obtained by error propagation. The diamond with error bar shows the experimental result from Ref. [26].

We now compare our results for $b_{3,1}^0$ and $b_{2,2}^0$ with the literature. The diagrammatic approach [23] yields $b_{3,1}^0 = 0.025$, which is within 2.5 standard deviations of our value, and $b_{2,2}^0/2 = -0.018$, which differs by a factor of about 1.5 (or many standard deviations) from our value. This comparison suggests that the convergence of the diagrammatic approach is slower for the (2,2) system than for the (3,1) system. The conjecture-based approach [24,25] yields $b_{3,1}^0 = 0.02297(4)$, which agrees within error bars with our value, and $b_{2,2}/2 = -0.0309(1)$, which differs by about a factor of 3 from our value.

Conclusion.—This Letter presented the PIMC determination of the fourth-order virial coefficient of the trapped unitary two-component Fermi gas. Our extrapolated infinite temperature result was found to agree with experiments within error bars, which, to the best of our knowledge, is the first numerical confirmation of the experimental determination of b_4. The customized PIMC scheme, which allows for the treatment of Fermi gases with zero-range interactions, can be applied to a variety of other situations.

Since the zero-range density matrix can be constructed for arbitrary s-wave scattering length a_s, the scheme can be used to study the finite-temperature characteristics of the BEC-BCS crossover of few-body Fermi gases. Moreover, the algorithmic developments can be integrated into PIMC ground state calculations, providing a viable alternative to basis set expansion approaches.

We are grateful to Kevin M. Daily for valuable correspondence, to Xiangyu Yin for thoughtful comments on the Letter, and to Yvan Castin for correspondence related to Refs. [25] and [50]. Support by the National Science Foundation (NSF) through Grant No. PHY-1415112 is gratefully acknowledged. This work used the Extreme Science and Engineering Discovery Environment (XSEDE), which is supported by NSF Grant No. OCI-1053575, and the WSU HPC.

Note added.—Recently, Endo and Castin revised their conjecture presented in Ref. [25]. The new calculation yields $b_4^0 = 0.00775(10)$, $b_{3,1}^0 = 0.02297(4)$, and $b_{2,2}^0/2 = -0.0152(1)$ [50].

[1] C. J. Pethick and D. G. Ravenhall, Annu. Rev. Nucl. Part. Sci. **45**, 429 (1995).
[2] P. A. Lee, N. Nagaosa, and X.-G. Wen, Rev. Mod. Phys. **78**, 17 (2006).
[3] J. Bardeen, L. N. Cooper, and J. R. Schrieffer, Phys. Rev. **106**, 162 (1957).
[4] R. B. Laughlin, Phys. Rev. Lett. **50**, 1395 (1983).
[5] P. Fulde and R. A. Ferrell, Phys. Rev. **135**, A550 (1964).
[6] A. I. Larkin and Yu. N. Ovchinnikov, Zh. Eksp. Teor. Fiz. **47**, 1136 (1964).
[7] A. I. Larkin and Yu. N. Ovchinnikov, Sov. Phys. JETP **20**, 762 (1965).
[8] S. Giorgini, L. P. Pitaevskii, and S. Stringari, Rev. Mod. Phys. **80**, 1215 (2008).
[9] I. Bloch, J. Dalibard, and W. Zwerger, Rev. Mod. Phys. **80**, 885 (2008).
[10] C. Chin, R. Grimm, P. Julienne, and E. Tiesinga, Rev. Mod. Phys. **82**, 1225 (2010).
[11] H. Heiselberg, Phys. Rev. A **63**, 043606 (2001).
[12] T.-L. Ho, Phys. Rev. Lett. **92**, 090402 (2004).
[13] K. Huang, *Statistical Mechanics* 2nd ed (Wiley, New York, 1987).
[14] T.-L. Ho and E. J. Mueller, Phys. Rev. Lett. **92**, 160404 (2004).
[15] X.-J. Liu, Phys. Rep. **524**, 37 (2013).
[16] X.-J. Liu, H. Hu, and P. D. Drummond, Phys. Rev. Lett. **102**, 160401 (2009).
[17] D. B. Kaplan and S. Sun, Phys. Rev. Lett. **107**, 030601 (2011).
[18] X. Leyronas, Phys. Rev. A **84**, 053633 (2011).
[19] S. Nascimbene, N. Navon, K. Jiang, F. Chevy, and C. Salomon, Nature (London) **463**, 1057 (2010).
[20] Y. Castin and F. Werner, Can. J. Phys. **91**, 382 (2013).
[21] C. Gao, S. Endo, and Y. Castin, Europhys. Lett. **109**, 16003 (2015).
[22] D. Rakshit, K. M. Daily, and D. Blume, Phys. Rev. A **85**, 033634 (2012).
[23] V. Ngampruetikorn, M. M. Parish, and J. Levinsen, Phys. Rev. A **91**, 013606 (2015).
[24] S. Endo and Y. Castin, Phys. Rev. A **92**, 053624 (2015).
[25] S. Endo and Y. Castin, arXiv:1512.06543v1.
[26] M. J. H. Ku, A. T. Sommer, L. W. Cheuk, and M. W. Zwierlein, Science **335**, 563 (2012).
[27] A. Comtet, Y. Georgelin, and S. Ouvry, J. Phys. A **22**, 3917 (1989).
[28] J. McCabe and S. Ouvry, Phys. Lett. B **260**, 113 (1991).
[29] D. M. Ceperley, Rev. Mod. Phys. **67**, 279 (1995).
[30] M. Boninsegni, J. Low Temp. Phys. **141**, 27 (2005).
[31] Y. Yan and D. Blume, Phys. Rev. A **91**, 043607 (2015).
[32] L. H. Thomas, Phys. Rev. **47**, 903 (1935).
[33] E. Braaten and H.-W. Hammer, Phys. Rep. **428**, 259 (2006).
[34] D. S. Petrov, Phys. Rev. A **67**, 010703 (2003).
[35] G. V. Skorniakov and K. A. Ter-Martirosian, Zh. Eksp. Teor. Fiz. **31**, 775 (1956), [Sov. Phys. JETP **4**, 648 (1957)].
[36] M. Takahashi and M. Imada, J. Phys. Soc. Jpn. **53**, 963 (1984).
[37] D. M. Ceperley, in *The Proceedings of the Les Houches Summer School, Session 56, Strongly Interacting Fermions and High T_c Superconductivity*, edited by B. Doucot and J. Zinn-Justin (Elsevier, Amsterdam, 1995), p. 427.
[38] E. Y. Loh, J. E. Gubernatis, R. T. Scalettar, S. R. White, D. J. Scalapino, and R. L. Sugar, Phys. Rev. B **41**, 9301 (1990).
[39] R. Stratonovich, Sov. Phys. Dokl. **2**, 416 (1957).
[40] D. Ceperley and B. Alder, Science **231**, 555 (1986).
[41] K. Huang and C. N. Yang, Phys. Rev. **105**, 767 (1957).
[42] X.-J. Liu and H. Hu, Phys. Rev. A **82**, 043626 (2010).
[43] K. M. Daily and D. Blume, Phys. Rev. A **85**, 013609 (2012).
[44] The explicit expressions for $b_{n_1,n_2}^{\mathrm{ref}}$ with $n_1+n_2=4$ read $b_{3,1}^{\mathrm{ref}} = -b_3 Q_{1,0} - 2b_2 Q_{2,0}$ and $b_{2,2}^{\mathrm{ref}} = -2b_3 Q_{1,0} - 2(b_2)^2 Q_{1,0} - 2b_2 (Q_{1,0})^2$.
[45] The Supplemental Material at http://link.aps.org/supplemental/10.1103/PhysRevLett.116.230401 contains (i) a summary of the literature values of the fourth-order virial coefficient, (ii) information on the pair product approximation and the two-body density matrix for zero-range interactions, and (iii) PIMC simulation details and tables containing selected raw data.
[46] For a simulation of finite length l, the standard deviation would not be following a Gaussian distribution, implying that the standard deviation would not decrease as $1/\sqrt{l}$ with increasing simulation length l.
[47] For the (2,2) system, e.g., $\mathcal{A}$ reads $(1 - P_{12} - P_{34} + P_{12}P_{34})/4$, where P_{ij} permutes the coordinates of particles i and j.
[48] S. A. Chin, Phys. Rev. E **91**, 031301(R) (2015).
[49] Y. Yan and D. Blume, Phys. Rev. A **90**, 013620 (2014).
[50] S. Endo and Y. Castin, arXiv:1512.06543v2.